HYDROLOGICAL PROCESSES
Hydrol. Process. (2016)
Published online in Wiley Online Library
(wileyonlinelibrary.com) DOI: 10.1002/hyp.10994

Rapid recharge of fresh water to the halite-hosted brine aquifer of Salar de Atacama, Chile

David F. Boutt,[1]* Scott A. Hynek,[2] Lee Ann Munk[3] and Lilly G. Corenthal[1]

[1] *Department of Geosciences, University of Massachusetts-Amherst, Amherst, MA, USA*
[2] *Earth and Environmental Systems Institute, Pennsylvania State University, University Park, PA, USA*
[3] *Department of Geological Sciences, University of Alaska-Anchorage, Anchorage, AK, USA*

Abstract:

We document, analyse, and interpret direct and rapid infiltration of precipitation to the southern margin of the Salar de Atacama halite-hosted brine aquifer during two intense precipitation events in 2012–2013. We present physical, geochemical, and stable and radioactive isotope data to detail this influx of water. The two events differ distinctly in the mechanisms of recharge. The 2012 event did not produce direct precipitation onto the salar surface, while the 2013 event did. Both events are recorded by abrupt changes in head in observation wells along the halite aquifer margin. Spatially distributed water levels rose by over 30 cm during the larger 2013 event consistent with remotely sensed observations of surface water extent. The lithium concentration and stable isotopic composition of water indicate dilution of brine and dissolution of salt with fresh water. Tritium measurements of precipitation, surface water, and groundwater all indicate modern influx of water to the halite aquifer along the southern margin. We extend these observations by examining the response of the halite aquifer as a whole to precipitation events during the period of 2000–2010. This study suggests that local recharge to the aquifer during sporadic precipitation onto the halite nucleus is an important component of the modern water budget in this hyper-arid environment. The rapid dissolution and salinization along the southern margin of the salar halite nucleus are aided by such precipitation events contributing a modern fresh water component to the water budget of the economically valuable lithium-rich brine. Copyright © 2016 John Wiley & Sons, Ltd.

KEY WORDS Salar de Atacama; halite; recharge; stable isotopes; tritium; Chile

Received 5 December 2015; Accepted 15 August 2016

INTRODUCTION

A salar, or playa, is a topographically closed (e.g. endorheic) intracontinental basin with a negative water balance for more than half the year that has accumulated evaporite minerals in the valley floor due to groundwater discharge (Rosen, 1994). Mature salars containing thick halite sequences host heterogeneous aquifers with variable fluid densities (Houston *et al.*, 2011). Salars accumulate evaporite minerals in the valley floor when potential evapotranspiration (ET) exceeds precipitation (Eugster, 1980); both the accumulation of evaporite minerals and the water table of a salar reflect a balance of water recharge and discharge (Rosen, 1994; Tyler *et al.*, 2006). Sources of inflow water to salars include surface waters and local and regional groundwater recharged by modern precipitation, draining groundwater storage, and hydrothermal fluids (Rosen, 1994). Determining the relative importance of the distinct hydrologic processes responsible for modern recharge/discharge of water (such as regional groundwater flow, local precipitation, and ET) within the basin floor is critical to understanding the sustainability and impact of groundwater pumping, resource extraction, and the resulting impacts on sensitive ecosystems.

One such closed basin, the Salar de Atacama (SdA), is a significant topographic depression that lies adjacent to the Altiplano–Puna plateau of the Central Andes (Figure 1). The topographic watershed encompasses an area over 17 000 km^2. The valley floor, at an elevation of 2300 m, is closed by the substantial topography of the Andean Cordillera (>5500 m) to the north, south, and east and Cordillera de Domeyko (>3500 m) to the west (e.g. Reutter *et al.*, 2006). Since the late Miocene, over 1800 km^3 of halite has accumulated in the Salar nucleus that hosts brine with some of the highest known concentrations of lithium (Munk *et al.*, 2016). The dominant halite-hosted brine aquifer is ringed by a zone characterized by salt precipitates (carbonate, gypsum, and halite) at the surface where inflowing water quickly evolves from low total dissolved solids to brackish and brine concentrations (herein called a transition zone).

*Correspondence to: David F. Boutt, Department of Geosciences, University of Massachusetts-Amherst, Amherst, MA, USA.
E-mail: dboutt@geo.umass.edu

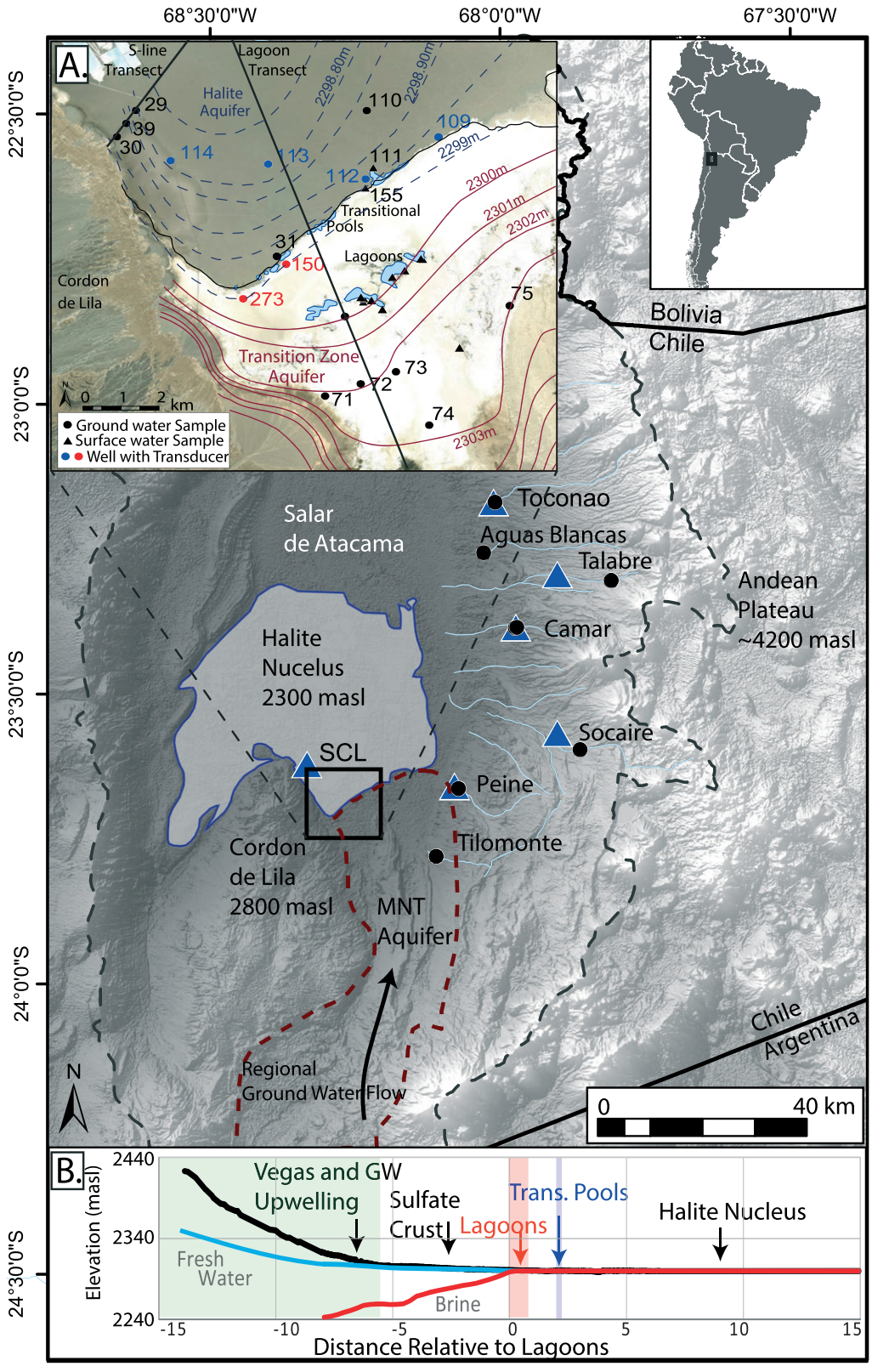

Figure 1. Location map of study region showing topographic watershed (dashed line), international boundaries (solid lines), and hydrographic features (streams in light blue) and data collection stations (the black dots are the stream gauging stations; the blue triangles are the meteorological stations). The boxed area shows the specific study area showing surface water (diamonds) and groundwater (circles) sampling and monitoring locations with contours of fresh/brackish water (red lines – 1-m contour interval) and brine (blue dashed lines – 0.05-m contour interval)

Evaporite sequences have also been identified in cores up to 90-m deep in this transition zone region (Munk *et al.*, 2016). The brine in the halite aquifer (assumed to have substantial permeability down to ~30 m; Houston *et al.*, 2011) is currently exploited for lithium and potassium resources. Understanding the sources and nature of groundwater recharge to the basin underlies many societal and scientific questions in the region. Debates regarding the amount of brine resource in place and the impacts of brine extraction on surrounding sensitive regions are ongoing. Constraining the processes that dominate the paleo and modern hydrologic budgets of these sensitive aquifers is critical towards placing reliable and bounded estimates of recharge for water supply and resource sustainability. In particular, prior to this study, very little effort has been put forth to document and understand the role of modern precipitation in the water budget.

Current process-based conceptual models of recharge to brine aquifers (e.g. SQM SA *et al.*, 2004; Tyler *et al.*, 2006; Salas *et al.*, 2010) suggest that precipitation on and direct local recharge to the aquifer comprise a small component of the total overall water budget with high-elevation sources being the source of recharge to basin floors (Magaritz *et al.*, 1990; Montgomery *et al.*, 2003; Houston, 2007; Houston, 2009; Johnson *et al.*, 2010). The mechanisms by which water moves through transition zones and into the halite aquifer are poorly understood; the potential for water to traverse the transition zones is limited by the strong ET fluxes. In this contribution, we document direct and rapid infiltration of precipitation to the southern margin of the SdA halite-hosted brine aquifer during two intense precipitation events in 2012–2013. We present physical, geochemical, and stable and radio-isotopic data to detail this influx of water. The two events differ in the mechanisms of recharge. The 2012 event is believed to have not produced direct precipitation onto the salar surface, while the 2013 event did rain on the salar. Both events are recorded by abrupt changes in head in observation wells in the salar margin. Similar water level changes across the whole halite nucleus were observed for 2001 and 2002 precipitation events. Water levels rose by over 30 cm during the large event and are spatially distributed over an area of 300 km^2. Tritium measurements of precipitation, surface water, and groundwater all support varying degrees of influx as do fluctuations in lithium concentrations. This evidence suggests that local recharge to this portion of the aquifer during infrequent but consistent precipitation onto and adjacent to the salar is an important component of the modern water budget of the halite aquifer. The rapid dissolution and salinization of the margin of the salar nucleus are aided by such precipitation events and contribute modern water (although lithium poor) to the brine aquifer.

SALAR DE ATACAMA AND THE TRANSITION ZONE

The SdA is characterized by a hyper-arid to arid climate due to its location under the subtropical high pressure zone, the presence of the cold Humboldt Current off the Pacific coast, and the Andean Cordillera acting as an orographic barrier to precipitation (Hartley and Chong, 2002). There is significant inter-annual variability in rainfall patterns; however, the majority of precipitation occurs during the austral summer and during wetter La Niña years (Garreaud *et al.*, 2003; Houston, 2006b). Infrequent high-intensity rainfall events play an important role in recharging groundwater based on observations in alluvial fans (Houston, 2002). There is a strong orographic effect on precipitation. On the Salar surface, average annual precipitation averages only 16 mm/year (Sociedad Chilena de Litio Ltda, 2009), while areas over 5000 m a.s.l. within the topographic watershed may receive over 300 mm/year of precipitation (Bookhagen and Strecker, 2008). Typical of global arid regions, precipitation likely only recharges the groundwater system in areas that receive over 120 mm/year of annual average precipitation (e.g. Scanlon *et al.*, 2006; Houston, 2007; Houston, 2009). According to the regional relationship for precipitation as a function of elevation (Houston, 2006a), >120 mm/year of precipitation only occurs above ~3900 m a.s.l.. The majority of the SdA topographic watershed is below 3900 m a.s.l., suggesting that these areas receive little significant modern groundwater recharge. Furthermore, the thickness of the vadose zone in the lateral zones of these aquifers (can reach >100-m thick) suggests that higher-elevation zones both within and adjacent to the topographic watershed are important sources of recharge (Anderson *et al.*, 2002; Rissmann *et al.*, 2015). Areas where the water table is at or near the ground surface and the aquifer maintains a closer physical hydraulic connection to areal precipitation, such as the SdA transition zone or higher-elevation salars and lakes, are the exception to these recharge–precipitation relationships.

Geology and hydrogeology

The modern mature salar system of SdA spans a surface area of approximately 3000 km^2 and includes a halite nucleus over 1200-m thick (Jordan *et al.*, 2002, 2007). The gypsum and carbonate-dominated transition zones of the southern SdA between the alluvium and halite facies are up to 9-km long (parallel to groundwater flow) and 20-km wide (perpendicular to groundwater flow) (Figure 1). Regional inflow waters to the closed basin of SdA come from the north, east, and southern recharge areas with little to no recharge from the west. The Salar basin can be divided into two distinct

morphologic zones. North of the Tumisa Volcano, the eastern slope of the Salar basin is characterized by monoclinal folding blanketed by substantial ignimbrite deposits and alluvial fans [e.g. Jordan *et al.*, 2002; Reutter *et al.*, 2006]. South of the Tumisa Volcano, the older lithospheric Peine block, bounded by the north-south trending Peine Fault System to the west and Quebrada de Nacimiento Fault to the east, separates the Salar from the Andes [Ramirez and Gardeweg, 1982; Aron *et al.*, 2008].

In the southern SdA watershed (the main focus of this paper), groundwater generally flows from south to north through the southern Monturaqui and central Negrillar basins, discharging in the Tilopozo area at elevations between 2300 and 2310 m a.s.l. (Rissmann *et al.*, 2015). The Monturaqui–Negrillar–Tilopozo (MNT) aquifer is approximately 60-km long (N-S) bordered by the Andean volcanic arc and Altiplano–Puna plateau to the east and south and N-S trending basement anticlines of the Cordón de Lila range to the west (Figure 1). The area is characterized by active modern (Late Miocene–Pliocene to present) volcanism and strato-volcanoes including Socompa (~6600 m) and Pular (~6200 m). Volcanoes, ignimbrite deposits, lahars, and lava flows are all significant features and deposits within the area.

Approximately 3.2 m^3/s of shallow subsurface groundwater discharges to the margins of SdA calculated based on hydraulic gradients, general aquifer properties and Darcy's Law (Correnthal *et al.*, 2016). The *Direccion General de Aguas* (2013) estimates total streamflow to SdA is 1.6 m^3/s based on gage measurements. The sum of shallow groundwater and streamflow (4.8 m^3/s) discharging to the margins of SdA reasonably explains low estimates of ET (5.17–22.7 m^3/s) off the basin floor (Mardones, 1986; Kampf and Tyler, 2006). The majority of ET occurs from transitional zones along the edge of the halite nucleus, with evaporation rates up to 5.8 mm/day from the lagoons located in the margins on the south, east, and north. Almost no (<0.005 mm/day) water evaporates from the halite nucleus due to the high fluid density and low capillary rise potential of the halite (Mardones, 1986; Kampf and Tyler, 2006). Discharge from the MNT aquifer (located up-gradient of our study area) is estimated to be 0.4–0.9 m^3/s (Anderson *et al.*, 2002), which is about 10 to 20% of the overall inflow flux to SdA.

The transition zone hosts a broad aquifer system where a freshwater-brine interface (Figure 1A) serves to focus groundwater discharge towards the surface. Water discharging out of the MNT aquifer into the transition zone increases in total dissolved solids due to shallow subsurface evaporative processes, and salt cycling though the relative importance of the latter is poorly understood. Water comes to the surface in the form of ephemeral pools and ponds, where discharge rates exceed evaporative flux water accumulates in a series of perennial brackish lagoons. These federally protected lagoons host diverse flora and fauna that are currently poorly understood.

METHODS

Detailed methods are presented in the Supporting Information; abbreviated methods are presented in the succeeding texts.

Field sampling

Six surface and ground water sampling campaigns were undertaken between January 2012 and January 2014 forming the basis of the study. Field parameters were measured *in situ*, and water level measurements were taken at all groundwater sampling locations. During the January 2014 sampling event, synoptic measurements of water levels, temperature, and specific conductivity were taken from surface and ground water wells in the transition zone aquifer and halite nucleus. Surface water samples were collected with plastic syringes from streams, lagoons, and open pools. Shallow ground water samples were sampled with a peristaltic pump through polyethylene tubing, and conductivity was monitored until it stabilized prior to sampling. All wells in this study are shallow piezometers screened at or below the water table with maximum depths no greater than 10 m. All water samples collected for analysis of lithium, major cations and anions, and δ^2H–H_2O and $\delta^{18}O$–H_2O were passed through 0.45-μm syringe filters and stored in clean high-density polyethylene bottles. Samples for lithium and major cation analysis were acidified with ultra-pure nitric acid to $pH < 2$. Samples for tritium analysis were collected in clean 1-L high-density polyethylene bottles with minimal headspace, and caps were sealed with electrical tape.

Physical hydrology

Meterological and streamflow data (see site locations on Figure 1) were obtained from Chilean Dirección General de Aguas and one station maintained by the Sociedad Chilena de Litio (SCL)/Rockwood Lithium Inc. Synoptic water level measurements during 12–14 January 2014 form the basis of a water table contour map in the southeastern transition zone. Depth to water measurements at a 0.01-m resolution were converted to total hydraulic heads and referenced to mean elevation above sea level (m a.s.l.) by using survey data where available. Continuous data were logged from four sites in the halite aquifer and two sites in the margin of the transition zone aquifer. For brines with conductivities greater than 240 mS/cm, pressures were converted to heads by using

a constant density of brine of 1225 kg/m^3. Wells in the halite nucleus have electrical conductivity profiles that reveal no stratification.

Remote sensing

Thirty-metre-resolution Landsat imagery at quarterly increments from years 2003 to 2014 are analysed for water coverage extent. Polygons of the area of lagoons and transitional pools were manually digitized, and surface areas are calculated in square metres. A second interpreter digitized ~3% of the images processed, and the calculated differences in areas were within 5% of each other on average.

Elemental and stable isotope geochemistry

Fluid samples were shipped to the University of Alaska Anchorage where all chemical analyses were performed. Samples were diluted gravimetrically, and lithium was analysed on an Agilent 7500c inductively coupled plasma–mass spectrometry following standard methods. The isotopic composition of water molecule was measured by wavelength scanned cavity ring-down spectrometry (Picarro L-1102i wavelength-scanned cavity ring down spectroscopy); samples were vaporized at 120 °C (150 °C for higher salt content waters). Long-term averages of internal laboratory standard analytical results yield an instrumental precision of 0.86‰ for δ^2H and 0.11‰ for δ^{18}O.

Tritium

Tritium (^{3}H) data for all samples were generated at the Dissolved and Noble Gas Laboratory, University of Utah, where 0.5-L aliquots were distilled, degassed in stainless steel vessels, and sealed in vacuum. Tritium concentrations were measured by using helium in growth (Clarke *et al.*, 1976); helium-3 concentrations are then measured on a MAP215-50 magnetic sector mass spectrometer by using an electron multiplier. Tritium data are reported in tritium units (TU) present in the sample on the sampling date, where 1 TU is equivalent to one tritium atom per 10^{18} hydrogen atoms (^{3}H/H * 10^{18}).

RESULTS

February 2012 and 2013 precipitation events

The two precipitation events at the focus of this paper are similar in magnitude and duration to events in the 30-year records of precipitation in the region and represent characteristic conditions. Event 1 was larger in magnitude than Event 2 at Peine despite no measureable precipitation recorded at the SCL precipitation gauge (Table I). Event 2 delivered more precipitation to the salar surface than what was recorded at the Peine station. The 2000–2014 precipitation measurements from both gauges (Figure 2) display no systematic correlation between precipitation, while there is strong correlation between monthly occurrence. The maximum monthly rainfall probability distribution at Peine has a potential 7-year and 2-year return period for events 1 and 2, respectively (Figure 3). The observed responses of both events include head changes in wells, flooding of low-lying regions adjacent to the halite aquifer, changes in the elemental and isotopic compositions of brine in the halite aquifer, and measurable changes in the size and extent of surface ponding in the transition zone.

Table I. Dates and magnitude of precipitation events recorded at the DGA Peine and SCL plant precipitation gauges

	DGA Peine precip. (mm)	*SCL plant (mm)*
Date	*Event 1*	
2/7/2012	4.5	0
2/8/2012	0.5	0
2/9/2012	18.5	0
2/10/2012	6	0
2/11/2012	4	0
2/12/2012	4	0
Total	32.5	0
Date	*Event 2*	
2/5/2013	0.5	0
2/6/2013	0.9	0
2/7/2013	11.5	24
2/8/2013	0.1	5.5
Total	13	29.5

Remote sensing of lagoon and transitional pool extents

Two major surface water features in the transition zone and halite margin are brackish lagoons and brine

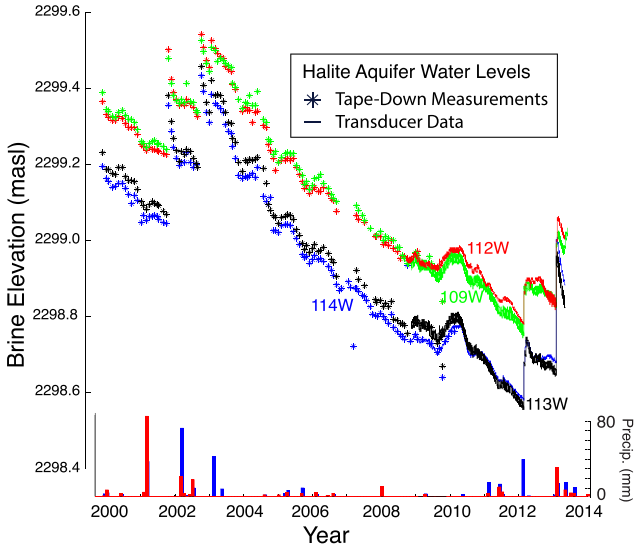

Figure 2. Tape down (coloured symbol) and pressure transducer (solid line) hydraulic head measurements for four wells screened in the halite aquifer with precipitation events recorded at the Peine Dirección General de Aguas (DGA) station (red) and at the SCL plant (blue)

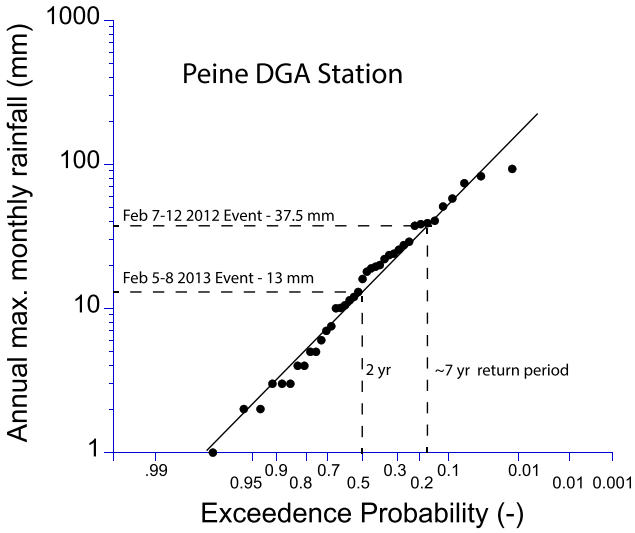

Figure 3. Exceedance probability plot for maximum monthly precipitation at the DGA Peine station from 1974 to 2014. Amounts and recurrence intervals for precipitation events subject of this study

transitional pools (blue polygons on inset in Figure 1). Figure 4 presents photos from site 111 looking south over the pools towards lagoons and transition zone. The photo from 14 January 2013 was almost a year after the February 2012 event and prior to the February 2013 event. Little surface water is observable in the pools at this period, and surface morphology (flat white salt crust) suggests re-precipitation of salts. The 18 May 2013 photo documents a significant growth of pools after both the February and May 2013 precipitation events, estimated depth of water is up to 0.5 m. The 12 January 2014 photo documents a significant reduction in total pool area (some pockets of brine appear on the right of the image) and re-precipitation of fresh (white) evaporite minerals. It is clear that the existence and extent of the pools are strongly correlated with local precipitation events and water is quickly evaporated and/or infiltrated.

We examine the relationship between surface water areal extent and precipitation events by using satellite imagery of the transition zone. Figure 5 presents remote sensing-based estimates of transitional pools (A) and lagoon areas (B) from 2003 to 2014. Throughout this period, the transitional pool area remains relatively small compared with brackish lagoons. The lagoons demonstrate a distinct seasonal change in area consistent with increases and decreases in open water evaporation rates driven by solar insolation (Salas *et al.*, 2010; Ortiz *et al.*, 2014). We have measured seasonal fluctuations in major element, lithium, and δ^2H–H_2O and $\delta^{18}O$–H_2O, which are correlated with changes in relative size of the lagoons (Munk *et al.*, 2016). Maximum and minimum lagoon areas are rather consistent through this time, with a slight downward trend, and are not strongly influenced by precipitation events of 2012 and 2013. This behaviour is consistent with the conceptual model that the lagoon water of the southeast transition zone is dominated by discharge of regional groundwater flow that evaporates at a greater rate in the austral winter (with peak areal extents in months between early April and late July). The extent of transitional pools lacks this seasonality and is dependent on local precipitation events to replenish. The response of transitional pools to Event 1 is not strong. There was a slight increase in area that persisted throughout 2012. After Event 2, the pool area grows by 200% and reaches it largest areal extent after a small May 2013 event . The onset of the austral summer during late 2013 and early 2014 drives transitional pool areas back to pre-2012 levels. The dominant hydrologic processes (infiltration *vs* evaporative losses) resulting in the loss of water from the pools are not well constrained. What is clear is that the lagoons and transitional pools are distinct hydrologic elements that have unique sources of water and responses to precipitation events. We use physical hydrologic data collected during the 2012 and 2013 events to further constrain the hydrologic responses.

Physical hydrology

Physical water level response to precipitation events of 2012–2013 was captured in six wells equipped with

Figure 4. Photographs taken from the edge of the halite aquifer looking approximately south into the transition zone. Significant changes in the area of the transitional pools are observed in response to local precipitation events

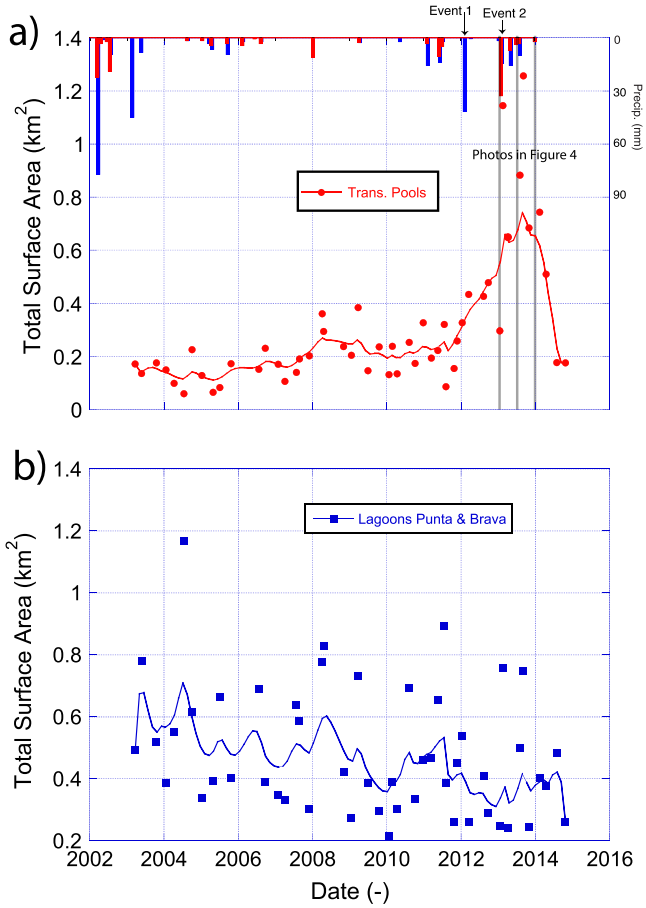

Figure 5. Time series of (a) transitional pools and (b) lagoon surface areas from 2003 to 2014 estimated from remote sensing fit with a 5-point moving average. A significant increase in pool area due to the large precipitation events in 2012 and 2013 is observed

pressure transducers (see inset in Figure 1). Figure 6 presents the time series of wells 109, 112, 113, and 114 screened in the halite aquifer with corresponding temperature measurements and monthly precipitation time series. Wells 150 and 273 screened in the transition zone aquifer only have data for Event 2 due to the lack of a barometric correction. We extract time to peak rise in water level (from midnight of the day of the precipitation event), magnitude of peak rise in water level, and slope of water level recession from transducer measurements for each location (Table II). Time to response of water level change is relatively fast (~3 days for Event 1 and ~0.5 day for Event 2). Event 2, which produced precipitation on the salar surface, caused the largest water rise and the fastest response of the water table. Water level response to recharge Events and 1 and 2 ranged from a minimum of 11 cm at well 273 and a maximum of 32 cm in well 114. While all monitored wells indicated a measured increase in water level, wells did not respond in a uniform manner. We extract distances of wells in the halite and transition zone aquifers to two potential sources of recharge, the Cordón mountain front and transitional pools, and plot observed head change for each precipitation event as a function of distance (Figure 7A). Wells screened in the halite aquifer have larger head changes closer to the Cordón mountain front. This trend is observed for both precipitation events. Conversely, when the magnitude of head change is compared with the distance from transitional pools (Figure 7B), the trend in magnitude shows that the head increases in the *further* wells are from the pools. Wells 150 and 273 screened in the transition zone aquifer do not follow the Cordón mountain front trend and suggest that the halite aquifer and transition zone aquifer are not hydraulically connected at the time scale of these responses. Head changes as a function of distance to the open pools suggest that they are not the sole source of recharge to the aquifer.

Results are consistent with a head change (perhaps from recharge) from precipitation events in the vicinity of the Cordón. To further evaluate this possibility, we use an analytical solution to the confined groundwater flow equation for a step change in head along a boundary (Pinder *et al.*, 1969) in a semi-infinite aquifer. The solution has the form of

$$\Delta H = H_o erfc\left(\frac{x}{2\sqrt{Dt}}\right)$$

where ΔH is the change in head at location x from the initial head change H_o at time t. D is the hydraulic diffusivity of the aquifer, which is the ratio of aquifer transmissivity (T) to confined storage (S). The appropriateness of using the confined solution to this aquifer is justified by the following: (1) the time-scale of response is fast enough such that the system essentially responds as a confined system (Reynolds, 1987) and (2) the inspection of the short-term response of the water levels presented in Figure 6 shows high-frequency oscillation consistent with earth tides that are characteristic of low storage confined aquifers (Rojstaczer and Agnew, 1989). The solution to this equation for initial head changes (H_o) at the Cordón mountain front is 0.19 and 0.35 m for Events 1 and 2, respectively. Initial head changes were adjusted to minimize the residual between the analytical solution (solid line in Figure 7) and the observations wells in the halite aquifer. A constant diffusivity, D, of 3e7 m^2/d (354.6 m^2/s) was used for both events. Assuming that this corresponds to a horizontal hydraulic conductivity of 1000 m/days (or 100 m/day) and a storage coefficient of 3.3e-04 (or 3.3e-05), both of which are consistent with pumping test results from

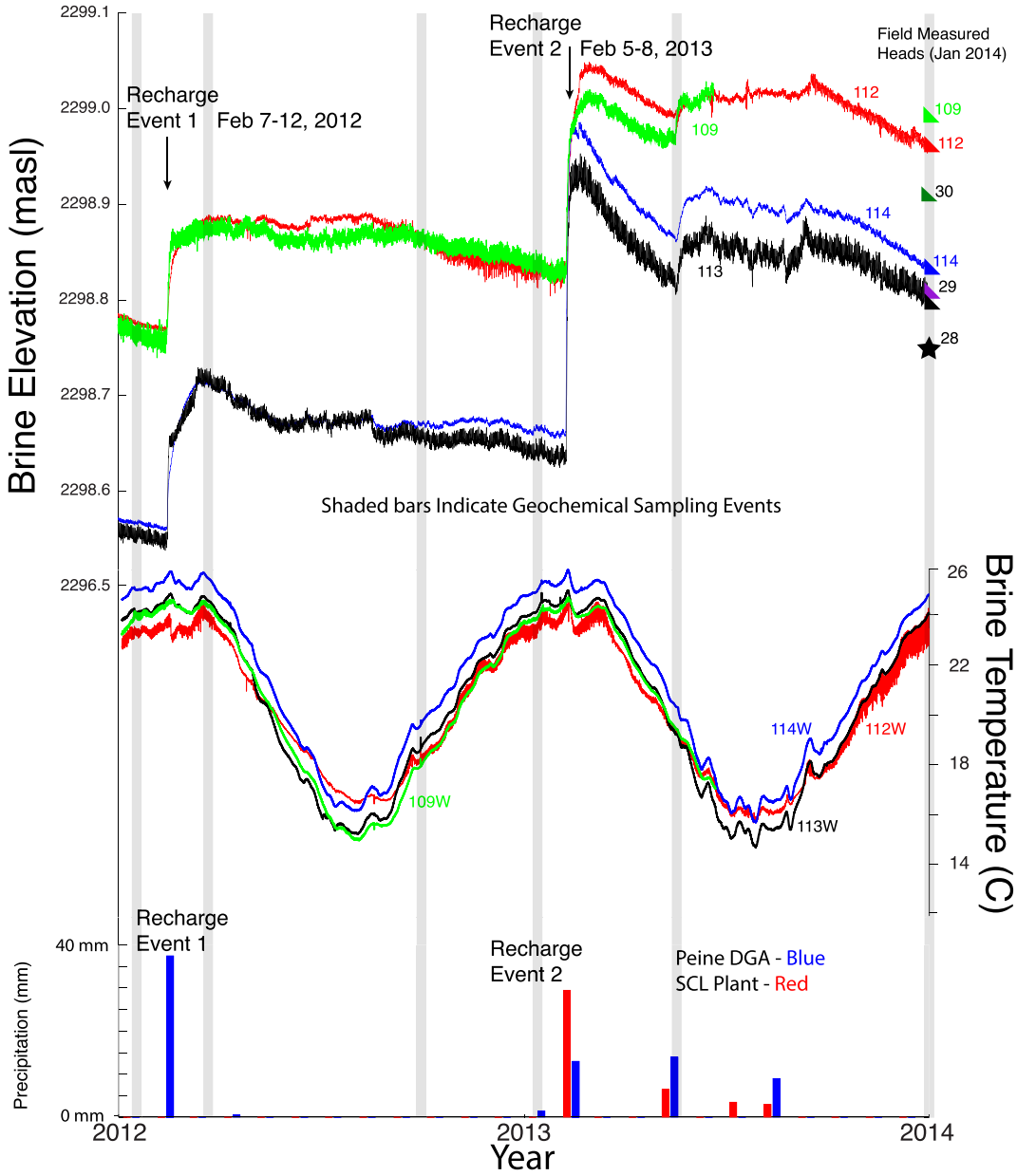

Figure 6. Pressure transducer hydraulic head and temperature measurements of wells screened in the halite aquifer during 2012–2014 recharge events and corresponding precipitation records at the DGA Peine station and the SCL precipitation station

wells in the halite aquifer (SQM SA *et al.*, 2004; Sociedad Chilena de Litio Ltda, 2009). The consistent trend and realistic range of hydraulic properties from the fit between analytical results and observations strongly suggest that the head changes observed in wells from both Events 1 and 2 are controlled by a hydraulic head rise in the vicinity of the Cordón. Importantly, this head rise is the propagation of a pressure wave from the boundary and does not necessarily reflect direct intrusion of modern water into the halite aquifer. We use geochemical and isotopic data to assess the degree of intrusion of modern water into the halite aquifer from potential sources of recharge.

Chemical composition of fluids

Lithium is a conservative ion and an abundant element, with a broad range of concentrations in the aqueous environments of interest (Table III). We therefore use its concentration to understand first-order responses of water composition to both seasonality and precipitation events. This is especially useful at the margin of the halite aquifer

Table II. Statistics and attributes of wells with recorded measurements of water level in response to recharge events

Well ID	Common name	Well depth (m)	Aquifer	Ground elevation (m)	Distance to transitional pools (km)	Distance to cordon (km)	Head response to: event 1 (m)	Event 2 (m)	Time to response (d) Event 1	Time to peak (d) Event 1	Time to response (d) Event 2	Time to peak (d) Event 2
112	TPB4	5.1	Halite	2299.960	0.2	6.1	0.12	0.21	3.2	46.6	0.4	17.3
113	TPB3	4.7	Halite	2299.899	2.0	3.8	0.15	0.29	3.4	35.1	0.6	7.8
114	TPB2	4.6	Halite	2299.908	3.0	1.4	0.17	0.32	3.1	36.8	0.3	7.2
109	TPB6	5.0	Halite	2300.131	0.1	8.2	0.12	0.18	2.5	38.6	0.6	17.9
150	TPDV8	2.0	TZ	2299.600	0.2	3.5	0.15	0.21	N/A	N/A	1.0	30.5
273	TPDV11	2.0	TZ	2299.800	0.2	2.8	0.11	0.14	N/A	N/A	1.0	30.9

where waters with wide ranges of lithium concentrations mix. We consider the major lithium reservoirs to be inflow, brackish, and brine fluids in this system as well as lithium contained in halite and its fluid inclusions. Concentrations of lithium in nucleus brines are on the order of thousands of mg/l, whereas we have measured lithium concentration in halite (lattice bound + fluid inclusions) on the order of tens of mg/l (averaging 40 mg/l over the length of a 60-m halite-dominated sediment core from the nucleus). When precipitation infiltrates either the transition zone or halite aquifers, complex processes of dissolution (halite) and mixing (brine) contribute lithium to the newly formed brine. This brine has a lithium concentration intermediate to rainwater (<1 mg/L) and nucleus brines, on the order of hundreds of mg/l. After precipitation events, waters exposed at the surface undergo evaporative concentration of lithium, further concentrating Li in the newly formed brine, but not achieving the highly economic concentrations of the nucleus brines.

Figure 8 illustrates the changes in lithium concentration in shallow groundwaters and waters exposed along the transition zone aquifer boundary and the halite aquifer during this study. There are significant changes in lithium concentrations over time, particularly following precipitation events. In general, lower lithium concentrations (<1000 mg/l) in brines occur in sample sites in the transition zone aquifer, transitional pools, and those closer to the halite aquifer edge, whereas those that are further into the halite aquifer have higher (>1000 mg/l) lithium concentrations. This is consistent with long-term lithium concentration data reported by SCL (unpublished data). However, the data presented here indicate that even the sites that are further into the halite aquifer have some variability over time.

Prior to Event 2, concentrations of lithium are generally constant to increasing with time at most sample site locations. Exceptions are sample sites 110 and 114, which indicate an increase (110) from 1206 to 1936 mg/l and a decrease (114) from 2488 to 587 mg/l post-precipitation Event 1. Additionally, after precipitation Event 1 and prior to precipitation Event 2, transitional pool sites (111 and 155) indicate an increase in lithium. At site 111, lithium concentration increases from 593 to 749 mg/l, and at site 155, lithium concentrations increase from 190 to 890 mg/l. These sites are open water locations where evaporative concentration is likely a strong control on the concentration of lithium.

After precipitation Event 2, all of the sampling locations indicate a decrease in lithium concentration. The last sampling event in the period of study indicates that the lithium concentrations increase after the decrease following precipitation Event 2. These trends in lithium concentration are consistent with the photographic and remote sensing observations recorded along the boundary

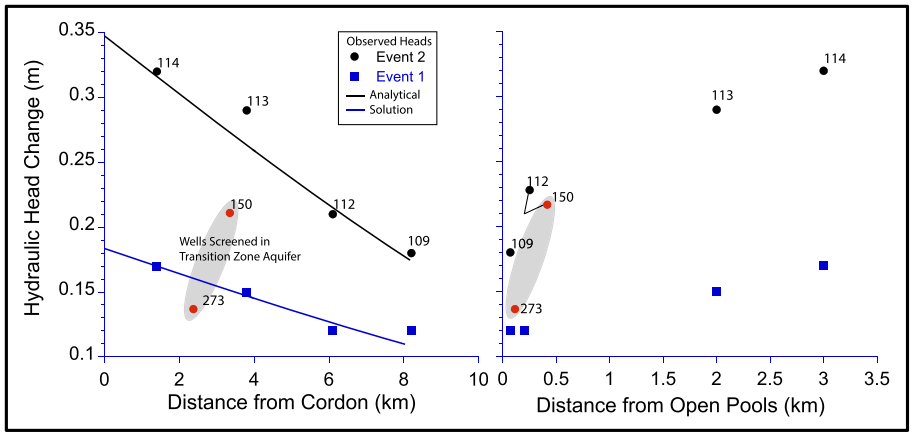

Figure 7. Rise in the altitude of the water table of wells screened in the halite aquifer in response to the two precipitation events described in the text. The red filled circles are the water table response in the marginal transition zone aquifer for only recharge Event 2

Table III. Geochemical and isotopic sampling locations and values for select wells in the study.

Sample ID	Latitude	Longitude	Common name	Location	Sample date	Specific conductivity (mS/cm)	Li (mg/l)	$\delta^{18}O$–H_2O ($^{o}/_{oo}$VSMOW)	$\delta^{2}H$–H_2O ($^{o}/_{oo}$VSMOW)
30	−23.68772	−68.31073	S1	Halite aquifer	3/10/2011	237.5	1150	−3.2	−36
30			S1	Halite aquifer	7/1/2012	235.4	1690	−1.4	−31
30			S1	Halite aquifer	6/4/2012	239.1	1658	−2.8	−36
30			S1	Halite aquifer	25/9/2012	235.8	1748	−1.2	−33
30			S1	Halite aquifer	14/1/2013	238.1	1688	−1.2	−29
30			S1	Halite aquifer	16/5/2013	241.5	662	−2.8	−35
30			S1	Halite aquifer	10/1/2014	240.2	1793	−2.6	−37
114	−23.69817	−68.24609	TPB2	Halite aquifer	10/1/2012	235.4	2489	0.0	−32
114			TPB2	Halite aquifer	6/4/2012	239.3	587	−3.0	−41
114			TPB2	Halite aquifer	26/9/2012	234.3	2725	−0.6	−35
114			TPB2	Halite aquifer	14/1/2013	184.6	2465	−2.4	−39
114			TPB2	Halite aquifer	18/5/2013	202.2	1753	−1.2	−34
114			TPB2	Halite aquifer	10/1/2014	237.5	3274	−0.5	−32
113			TPB3	Halite aquifer	10/1/2012	239.1	1090	6.6	0
113			TPB3	Halite aquifer	6/4/2012	240.6	1048	5.7	0
113	−23.69480	−68.27170	TPB3	Halite aquifer	26/9/2012	237.4	1017	6.1	−2
113			TPB3	Halite aquifer	14/1/2013	240.3	899	4.0	−7
113			TPB3	Halite aquifer	18/5/2013	230.0	1176	6.7	1
113			TPB3	Halite aquifer	14/1/2014	246.6	922	5.0	−6
112	−23.69857	−68.24658	TPB4	Halite aquifer	10/1/2012	240.6	721	13.7	26
112			TPB4	Halite aquifer	6/4/2012	240.8	1009	11.8	23
112			TPB4	Halite aquifer	26/9/2012	239.2	726	10.3	13
112			TPB4	Halite aquifer	14/1/2013	239.1	719	10.2	14
112			TPB4	Halite aquifer	18/5/2013	239.7	291	10.6	14
112			TPB4	Halite aquifer	13/1/2014	244.4	916	11.0	17
112			TPB4	Halite aquifer	18/8/2014	241.0	375	10.4	14
110	−23.68054	−68.24639	TPB5	Halite aquifer	10/1/2012	237.5	1206	7.5	0
110			TPB5	Halite aquifer	6/4/2012	238.3	1935	6.6	0
110			TPB5	Halite aquifer	26/9/2012	238.7	1187	7.4	2
110			TPB5	Halite aquifer	14/1/2013	237.4	1135	7.4	4
110			TPB5	Halite aquifer	18/5/2013	237.9	487	7.2	−1
110			TPB5	Halite aquifer	13/1/2014	241.1	1100	6.6	0
150	−23.72117	−68.26693	TPDV8	Transition zone aquifer	5/4/2012	240.2	1096	5.7	−2
150			TPDV8		29/9/2012	239.3	391	6.5	−1

Continues

Table III. (*Continued*)

Sample ID	Latitude	Longitude	Common name	Location	Sample date	Specific conductivity (mS/cm)	Li (mg/l)	$\delta^{18}O–H_2O$ ($^o/_{oo}$VSMOW)	$\delta^{2}H–H_2O$ ($^o/_{oo}$VSMOW)
				Transition zone aquifer					
150			TPDV8	Transition zone aquifer	14/1/2013	241.4	421	6.3	1
150			TPDV8	Transition zone aquifer	16/5/2013	239.3	184	7.3	3
150			TPDV8	Transition zone aquifer	15/1/2014	241.3	470	7.1	3
150			TPDV8	Transition zone aquifer	18/1/2014	238.0	244	6.5	1
155	−23.70098	−68.24660	N/A	Transitional pool	6/4/2012	238.2	190	11.2	18
155			N/A	Transitional pool	26/9/2012	243.9	576	17.8	43
155			N/A	Transitional pool	14/1/2013	173.8	895	15.4	36
155			N/A	Transitional pool	18/5/2013	238.9	163	−0.4	−36
155			N/A	Transitional pool	13/1/2014	231.7	735	13.3	26
155			N/A	Transitional pool	18/8/2014	221.7	595	12.5	26
111	−23.69565	−68.24459	N/A	Transitional pool	10/1/2012	244.0	593	12.6	20
111			N/A	Transitional pool	6/4/2012	227.8	2126	8.8	9
111			N/A	Transitional pool	26/9/2012	242.6	749	9.0	7
111			N/A	Transitional pool	14/1/2013	243.1	858	14.2	29
111			N/A	Transitional pool	18/5/2013	232.7	175	1.0	−32
111			N/A	Transitional pool	13/1/2014	211.8	740	9.0	10

of the transition zone aquifer and the halite aquifer, where there appears to be a dilution effect after precipitation Event 2 followed by a period of evaporation, salt precipitation, and a corresponding increase in lithium concentrations in the brine.

Stable isotopic composition of fluids

Stable isotopes of hydrogen and oxygen in water are excellent indicators of evaporative processes in salar environments and can be a useful tool for understanding the interaction of precipitation with surface and ground water that has undergone evaporation. A plot of $\delta^{2}H–H_2O$ *versus* $\delta^{18}O–H_2O$ presents data in a way that evaporation can easily be assessed relative to the global average precipitation (global meteoric water line). We present data in Figure 9 collected along a transect from up-gradient of the transition zone before the groundwater is impacted by evaporative processes. We consider these samples to reflect the composition of regional groundwater flow (orange diamonds) discharging out of the MNT aquifer system (Rissmann *et al.*, 2015). As this water moves through the transition zone aquifer (red open squares), it is strongly impacted by evaporation – as indicated by a trend off the meteoric water line at about 15° for a relative humidity of ~25% (Clark and Fritz, 1997). Because shallow groundwater flow rates are high and evaporative fluxes are minimized by overlying deposits, surface water features (lagoons and transitional pools) are more

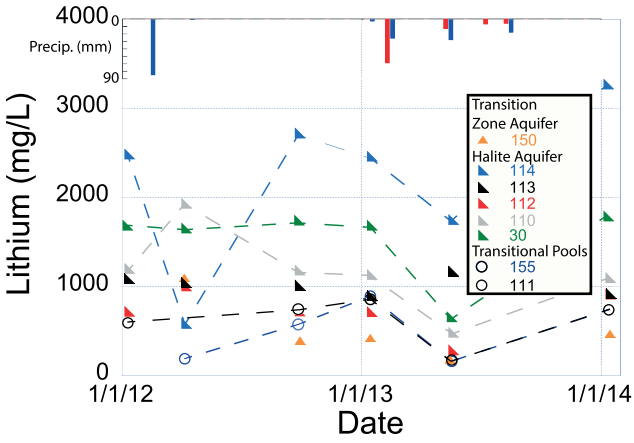

Figure 8. Time series of lithium concentration in samples from transitional pools and wells located in the transition zone and halite aquifer. Precipitation events shown for reference

evaporatively enriched. Thus, the lagoons show a wide range of evaporative enrichment in the heavy isotopes (grey triangles) dependent on the location of the samples relative to the main inflow location in the lagoon and when the sample was collected. The transitional pools at the margin of the halite nucleus (blue solid circles) show the highest degree of evaporative enrichment of all water samples. Curiously waters sampled in the halite aquifer (down-gradient of lagoons and transitional pools) show a large range of evaporative enrichment and cluster in

groups that document strong spatial variability that is persistent through the period of study (red-shaded ellipses). Over this interval, 14 monthly samples were taken in three locations in the lagoons and never found to be more evaporatively enriched than the transitional pools. Because the lagoons are strongly supported by consistent inflows of regional groundwater flow, water that is lost to evaporation is being constantly re-supplied with less evaporated water resulting in a water balance that controls the water depth and areal extent of the lagoons. Conversely, the transitional pools at the edge of the halite aquifer are supplied with water during precipitation events and become evaporatively enriched following a precipitation event because little to no inflow of less evaporated water (such as that from the lagoons) occurs between precipitation events.

The time series of δ^2H–H_2O (‰Vienna standard mean ocean water) are shown in Figure 10 for the same sample locations as presented in the lithium time series (Figure 8). The δ^2H values from the halite aquifer and transition zone aquifer are fairly consistent with time and show a small decrease in δ^2H–H_2O after the February 2012 event. Relative to lithium concentration, the stable isotopic composition of the transitional pool water has a strong response following the Event 2. First, it is depleted in heavy isotopes by addition of rainwater and becomes enriched by evaporation as documented by the January 2014 samples, which do not reach pre-February 2012 levels (e.g. 111). The time series data indicate a source of less evaporated water in open pools identified by more depleted isotopic compositions than lagoon water.

With a large number of sampling sites, we investigate spatial patterns in δ^2H–H_2O as an approach to identify water pathways through the transition zone into the halite aquifer. Figure 11 presents a coloured contoured map of average δ^2H–H_2O (‰ Vienna standard mean ocean water) of all groundwater sample sites in the transition zone. Down-gradient of the lagoons, water becomes increasingly evaporated with a majority of sample sites (260, 262, 245, and 242) depleted in δ^2H–H_2O with respect to average lagoon water. Solely based on the δ^2H data, it is difficult to tell if the water between the lagoons and the transitional pools is infiltrated pool water or highly evaporated lagoon water. The most evaporated waters in the halite aquifer exists at those sample locations closest to the transitional pools (sites 112 and 109 have the most positive δ^2H values). Because transitional pools are significantly more evaporated than the most evaporated lagoon water, this observation suggest that the water in the marginal halite aquifer is dominated by transitional pool water and not lagoon water. Highly evaporated water is present 3–4 km into the halite aquifer and is interrupted by less evaporated water adjacent to the Cordón mountain front. In fact, the isotopic composition of brine adjacent to the Cordón is less evaporated than the average lagoon water, suggesting that there is a source of recharge to the halite aquifer from the Cordón. This water recharges directly from the alluvial to the halite aquifer without a pronounced transition zone where it would spend time at the surface and acquire an evaporatively enriched δ^2H signal. Samples of brine in the halite aquifer towards the salar centre (Godfrey *et al.*, 2003) have δ^2H values of 0–5‰,

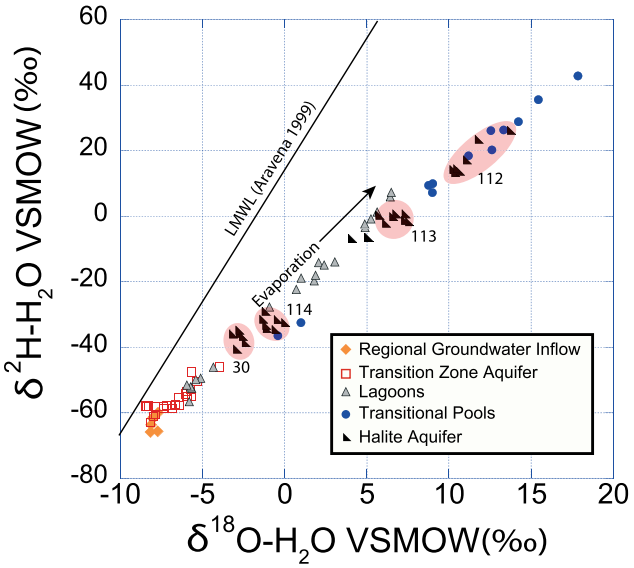

Figure 9. Stable isotope composition of surface and ground waters in the transition zone and halite aquifer. The shaded polygons represent the range of variability of a give sample halite aquifer sample site during the study period. The solid line defines the local meteoric water line

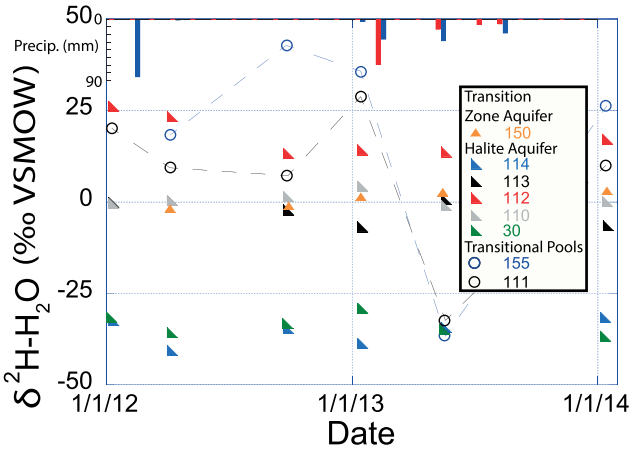

Figure 10. Time series during the study period of δ2H–H2O Vienna standard mean ocean water (VSMOW) of samples from transitional pools and wells located in the transition zone and halite aquifer. Precipitation events shown for reference

suggesting that the southwestern portion of the halite aquifer is dominated by water moving through the transitional pools. While δ^2H is a good tracer to identify mixing processes of water with distinctive isotopic compositions, it does not provide a complete picture of water movement or transit times.

Tritium content of fluids

Analyses of tritium (^3H) in waters of the transition zone are presented in Table IV. For inter-comparison of all samples collected, we decay tritium concentration from the time of sampling to 15 January 2015. These data, presented as $^3H^*$, permit analysis of spatial

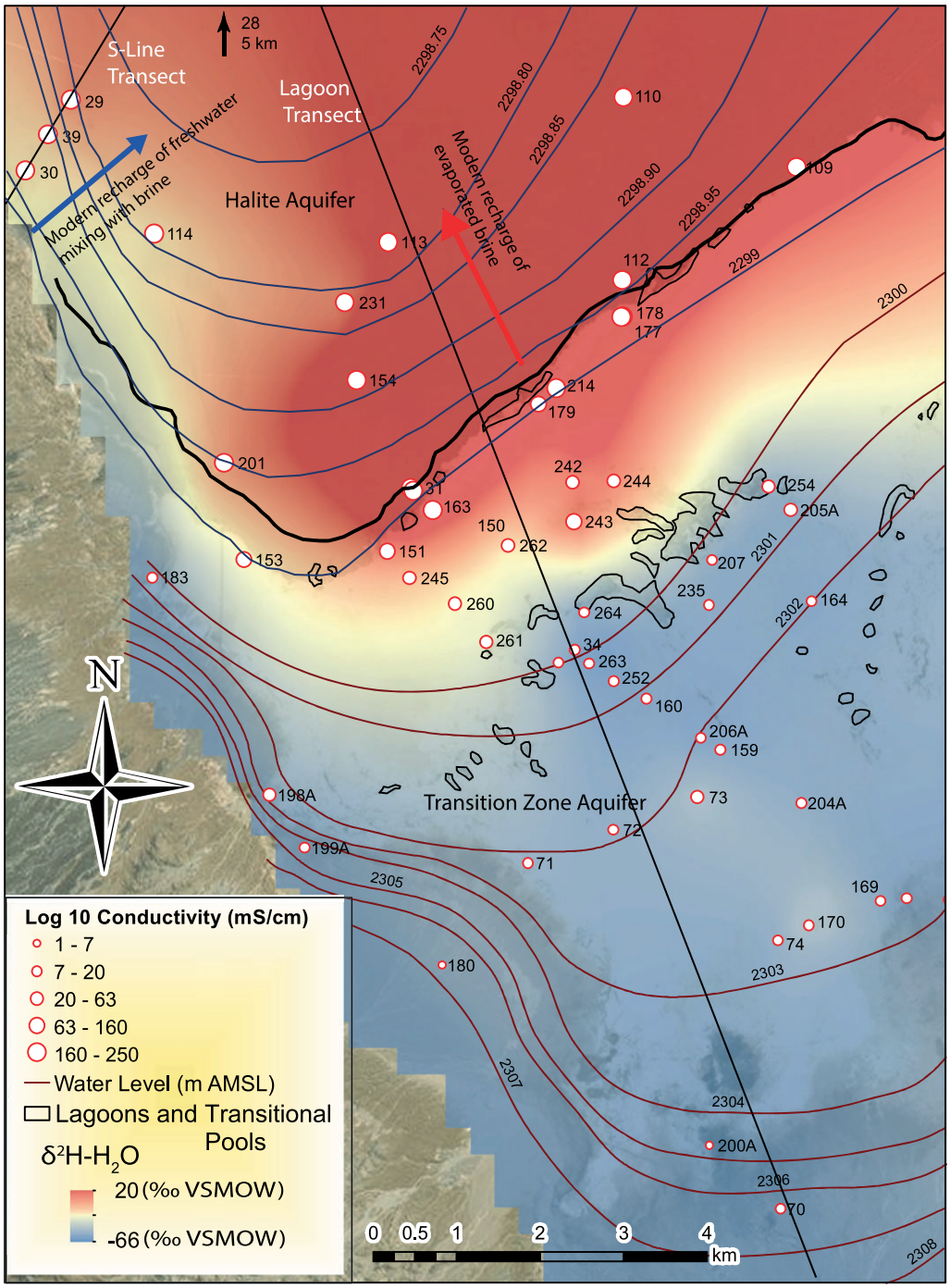

Figure 11. Coloured contour map of average δ2H–H2O VSMOW from all sampling events in the region of the transition zone and halite aquifers. Sample location symbols are sized by electrical conductivity of waters with a water table contour map of hydraulics measured in January 2014. Surface water features are indicated by open unfilled polygons

patterns that are not obscured by differences in the date of sampling. Additionally, we calculate for each sample R_{mod} (Figure 12), which is the ratio of sample tritium concentration in TU to our average precipitation value of 3.2 ± 0.6 TU (1σ). This estimate of the tritium concentration of modern precipitation is generated from five rain samples collected in the watershed during 2013 and 2014, we assume that this is representative of precipitation values from 1990 to present. These observations also agree with precipitation data presented by Houston (2002, 2007), though he chooses a higher value for modern precipitation, and are consistent with the summary provided by Herrera *et al.* (2006).

Having confidence in the ^{3}H of modern precipitation, we consider this same value to be representative of pre-1955 values as well. Background tritium of 3.2 ± 0.6 TU, recharged in 1955, would have 0.09–0.13 TU in January 2015. Groundwater recharge with background ^{3}H values in 1960, immediately prior to the bomb peak, would have 0.12–0.17 TU in January 2015. This is consistent with the wide range of samples that have ^{3}H* <0.15 TU; these samples can be confidently interpreted to have mean residence times in excess of 60 years. Although we have some evidence of *in situ* production of ^{3}H in what are presumably very old brines far from freshwater inflows (sample site 28), a potentially important consideration in Li-rich aquifers, the values measured support a cut-off of 0.15 TU for positive identification of modern water (Table IV and Figure S1 in the Supporting Information). Production of ^{3}H via neutron reactions in ^{6}Li is a consideration in the study environments but requires both high Li concentrations and a source of neutrons (e.g. cosmic rays or U/Th decay). The analysis of inflow water samples with ^{3}H concentrations, which are indistinguishable from 0.00 TU, suggests that *in situ* production of ^{3}H in freshwater aquifers is minimal, whereas the 0.15 TU cut-off proposed for modern water represents an absolute maximum value for *in situ* ^{3}H production in an extremely high Li environment (sample 28 Li concentration is ~1700 mg/l).

Tritium concentrations of discrete samples decayed to 15 January 2015 (^{3}H*) vary from 0.99 TU for waters in the transitional pools to 0.02 TU for inflowing regional groundwater. Average ^{3}H* values of inflow and transition zone waters are 0.20 ± 0.24 TU (1σ), and marginal halite aquifer brines are 0.55 ± 0.25 TU (1σ) compared with our measured modern precipitation value of 3.2 ± 0.6 TU (1σ). The higher average tritium concentration in marginal brine indicates a modern water component to the halite aquifer.

Where we have multiple tritium analyses of the same site during 2012–2013, we present them as time series of ^{3}H (TU) for wells in the transition zone aquifer, the halite aquifer, and transitional pools (Figure 13). Samples of ^{3}H for most sites are stable over time. Brine in the transitional pools varies most of any site with an increase in ^{3}H corresponding to the February 2013 precipitation event. Interestingly, ^{3}H concentration in the transitional pool decreases in the sample from January 2012 to September 2012. This decrease in ^{3}H is too rapid to result from radioactive decay and suggests that the water in the open pool represents a mixture of nucleus brine or lagoon water over that period. Site 30 also shows a similar trend during this time, which is not likely being diluted by lagoon water.

To investigate spatial variations in tritium concentrations without decaying them to 15 January 2015, and to facilitate estimates of mean residence times, we present average values of R_{mod} for surface water and groundwater sampling locations along two cross sections in Figure 12 (see Figure 11 for cross-section locations). Figure 12A shows the tritium values (R_{mod}) along a transect parallel to the regional flow path intersecting the lagoons and halite aquifer. Site 69 is the furthest up-gradient sample with a tritium result, and in general, these regional groundwaters (sites 69, 70, and 74) have little to no tritium (0.02–0.23 ^{3}H* TU), consistent with the conceptualization that the regional groundwater flow paths emerging from the MNT aquifer are long and reflect older groundwater. There is some evidence that the aquifer is age and salinity-stratified, and our sampling very near the water table is most likely to capture some component of modern water; however, the vast majority of water in this aquifer is considered pre-modern. Site 73 in the transition zone aquifer is the only sample of groundwater up-gradient of lagoons that contains appreciable tritium. The lagoons have 0.50–0.74 ^{3}H* TU (sites 35, 36, and 37), whereas a flowing borehole discharging brackish water into the lagoons (site 36A) has essentially no tritium (0.06 ^{3}H* TU). These results suggest that flow paths delivering water to lagoons are varied and consist of long and short residence time flow paths including the possibility of shallow subsurface runoff during wetter periods.

Brine samples in the halite aquifer show a rapid decrease of ^{3}H concentration with distance from the transitional pools (Figure 12A). We interpret this trend to suggest an infiltration of water from the transitional pools to the halite aquifer at minimum seepage velocities approaching 0.7 m/day. Velocities are approximated by assuming that the samples are along a single flow path and that the difference in ages calculated by using the average R_{mod} value are a function of lateral flow velocity towards the centre of the salar. This approach negates concern about lack of a historical ^{3}H input function (e.g. bomb peak) because it assumes that all study sites had the same recharge composition and the age difference between two laterally connected wells does not depend on the initial recharge value. Figure 12B depicts a transect of four tritium analyses (S-Line transect) that trends off

Table IV. Locations and values of tritium measurements.

Transect/Location	Sample ID	Collection	Latitude	Latitude	Elevation	Depth^	SC	^{3}H		^{3}H*	$R^{\#}_{mod}$
		date	(°N)	(°W)	(m)	(mbls)	mS/cm	(TU)	Error	15-Jan-2015	
Halite aquifer aquifer											
S Line/Lagoon Transect	28	6-Jan-2012	−23.6086	-68.2546	2304	2.0	233	**0.25**	0.02	*0.21*	*0.08*
S Line/Lagoon Transect	28	6-Jan-2012	*duplicate analysis of the same sample*				233	**0.24**	0.02	*0.20*	*0.07*
S Line/Lagoon Transect	28 - Shallow	7-Jan-2012	−23.6086	−68.2546	2304	2.5	233	**0.11**	0.08	*0.09*	*0.03*
S Line/Lagoon Transect	28 - Shallow	7-Jan-2012	*duplicate analysis of the same sample*				233	**0.17**	0.03	*0.15*	*0.05*
S Line/Lagoon Transect	28 - Medium	7-Jan-2012	−23.6086	−68.2546	2304	6.5	234	**0.15**	0.03	*0.13*	*0.05*
S Line/Lagoon Transect	28 - Deep	7-Jan-2012	−23.6086	−68.2546	2304	13.2	231	**0.13**	0.03	*0.11*	*0.04*
S Line Transect	29	7-Jan-2012	−23.6807	−68.3058	2306		232	**0.12**	0.06	*0.10*	*0.04*
S Line Transect	39	7-Jan-2012	−23.6842	−68.3083	2306		168	**0.12**	0.06	*0.10*	*0.04*
S Line Transect	30	3-Oct-2011	−23.6877	−68.3107	2306		237	**0.52**	0.03	*0.43*	*0.16*
S Line Transect	30	7-Jan-2012	−23.6843	−68.3090	2306		235	**0.66**	0.04	*0.55*	*0.20*
S Line Transect	30	25-Sep-2012	−23.6843	−68.3090	2306		236	**0.41**	0.03	*0.36*	*0.13*
S Line Transect	30	14-Jan-2013	−23.6843	−68.3090	2306		238	**0.38**	0.05	*0.34*	*0.12*
S Line Transect	30	16-May-2013	−23.6843	−68.3090	2306		242	**0.54**	0.04	*0.49*	*0.17*
Lagoon Transect	112	10-Jan-2012	−23.6986	−68.2466	2306		241	**1.17**	0.05	*0.99*	*0.36*
Lagoon Transect	112	26-Sep-2012	−23.6986	−68.2466	2306		239	**0.63**	0.04	*0.55*	*0.20*
Lagoon Transect	112	14-Jan-2013	−23.6986	−68.2466	2306		239	**0.59**	0.05	*0.53*	*0.18*
Lagoon Transect	112	18-May-2013	−23.6986	−68.2466	2306		240	**0.68**	0.07	*0.62*	*0.21*
Lagoon Transect	113	6-Apr-2012	−23.6948	−68.2717	2307		241	**0.59**	0.03	*0.50*	*0.18*
Lagoon Transect	113	26-Sep-2012	−23.6948	−68.2717	2307		237	**0.71**	0.03	*0.62*	*0.22*
Lagoon Transect	113	14-Jan-2013	−23.6948	−68.2717	2307		240	**0.68**	0.05	*0.61*	*0.21*
Lagoon Transect	113	18-May-2013	−23.6948	−68.2717	2307		230	**0.46**	0.20	*0.42*	*0.14*
Transitional pools											
Lagoon Transect	111	10-Jan-2012	−23.6956	−68.2446	2305		243	**1.17**	0.13	*0.99*	*0.36*
Lagoon Transect	111	26-Sep-2012	−23.6956	−68.2446	2305		244	**0.60**	0.04	*0.53*	*0.19*
Lagoon Transect	111	14-Jan-2013	−23.6956	−68.2446	2305		233	**1.11**	0.05	*0.99*	*0.34*
Lagoon Transect	111	18-May-2013	−23.6956	−68.2446	2305		212	**1.72**	0.17	*1.57*	*0.53*
Lagoons, transition zone aquifer, and inflow waters											
Lagoon Transect	150	29-Sep-2012	−23.7212	−68.2669	2308		239	**0.73**	0.04	*0.64*	*0.23*
Lagoon Transect	150	14-Jan-2013	−23.7212	−68.2669	2308		241	**0.55**	0.06	*0.49*	*0.17*
Lagoon Transect	150	16-May-2013	−23.7212	−68.2669	2308		239	**0.53**	0.05	*0.48*	*0.16*
Laguna La Brava B	35	3-Oct-2011	−23.7307	−68.2449	2307		93	**0.89**	0.05	*0.74*	*0.28*
Laguna La Brava A	36	3-Oct-2011	−23.7298	−68.2476	2305		86	**0.60**	0.07	*0.50*	*0.18*
Brava-borehole	36A	15-May-2013	−23.7302	−68.2468	2305		85	**0.07**	0.01	*0.06*	*0.02*
Laguna La Brava C	37	3-Oct-2011	−23.7330	−68.2420	2308		29	**0.60**	0.06	*0.50*	*0.19*
Lagoon Transect	69	12-Jan-2012	−23.8007	−68.2332	2324	15–17	3.9	**0.06**	0.04	*0.05*	*0.02*
Lagoon Transect	69	12-Jan-2012	*duplicate sample*					**0.03**	0.02	*0.02*	*0.01*
Lagoon Transect	70	12-Jan-2012	−23.7900	−68.2295	2316	6–10	15	**0.28**	0.05	*0.23*	*0.09*
Lagoon Transect	70	12-Jan-2012	*duplicate sample*					**0.10**	0.02	*0.08*	*0.03*

Continues

Table IV. (*Continued*)

Transect/Location	Sample ID	Collection	Latitude	Latitude	Elevation	Depth^	SC	^{3}H		^{3}H*	$R^{\#}_{mod}$
		date	(°N)	(°W)	(m)	(mbls)	mS/cm	(TU)	Error	15-Jan-2015	
Lagoon Transect	70	12-Jan-2012	*Reanalysis of the duplicate sample*					**0.08**	0.05	*0.07*	*0.03*
Lagoon Transect	73	12-Jan-2012	−23.7494	−68.2385	2309	~0.4	26	**0.69**	0.18	*0.58*	*0.21*
Lagoon Transect	74	12-Jan-2012	−23.7635	−68.2298	2310	~0.4	6.9	**0.03**	0.03	*0.03*	*0.01*
Precipitation samples, Andes, and El Salar											
Andean Rain	185	19-Jan-2013	−23.8374	−67.8534	3910		*0*	**4.19**	0.15	*3.75*	*1.30*
Salar Rain	187	20-Jan-2013	−23.6145	−68.0630	2318		*0*	**3.25**	0.26	*2.91*	*1.01*
Peine Rain	188	20-Jan-2013	−23.6818	−68.0673	2381		*0*	**3.23**	0.14	*2.89*	*1.00*
Peine Rain	190	17-May-2013	−23.6818	−68.0673	2381		*0*	**2.84**	0.10	*2.59*	*0.88*
Salar Rain	216	16-Jan-2014	−23.6633	−68.2926	2307		*0*	**2.64**	0.11	*2.50*	*0.82*

^ mbls, metres below land surface; depth, sampling depth.
*Tritium concentration decayed to 15 January 2015 to facilitate inter-comparison of data.
Ratio of TU value to the estimated value for modern precipitation; $R_{mod} > 1$ is highly unlikely unless the water was recharged during the bomb peak.
Italics for the two rightmost columns denote that these parameters are derived from measured values (shown in bold).

the Cordón mountain front and terminates in the halite aquifer at site 28. As opposed to the Lagoon transect, the S-Line transect does not have a large source of regional groundwater flow or even a transition zone. Tritium was only detected in significant concentrations at site 30 and quickly decays to background levels. Using this trend we estimate a seepage velocity of 0.10 m/day. In this scenario, dissolution of salt by fresh inflow water should not affect the ^{3}H content of the fluid, nor influence the estimated seepage velocity; however, mixing of inflow water with brine would dilute the ^{3}H content and reduce estimates of seepage velocity. We therefore interpret the 0.10 m/day seepage velocity off the Cordón as a minimum value, but without strong evidence for mixing of brine and inflow water at this location, we deem it realistic. The presence of significant ^{3}H (0.52 and 0.66 TU) in samples from site 30 prior to the February 2012 precipitation event suggests that a consistent source of young inflow water from the Cordón to the salar exists irrespective of precipitation events. Rapid infiltration and mixing are therefore not required to generate the observed ^{3}H values, and the estimated seepage velocity is reasonable. Consistent with the physical hydrologic data, and supported by stable isotopic data (cf. Figure 11), we detect a source of modern unevaporated recharge off the Cordón mountain front into the halite aquifer. Figure 12C depicts the hydraulic gradients along the transect based on head measurements taken during January 2014. The contours of hydraulic head are also shown in Figure 12. While the gradients are very small (mm/km), the hydraulic data indicate a potential for fluid flow in the halite aquifer from the transitional pools and Cordón mountain front towards the core of the halite aquifer, providing a critical physical basis for our interpretation of seepage velocities along these transects (Figure 14).

DISCUSSION

Conceptual model of the hydrologic functioning of the transition zone

The water discharging in the vicinity of the Punta/Brava lagoon (See Figure 1) complex flows along long flow paths discharging from the MNT aquifer system. As the water enters the Tilopozo region, it begins to undergo a physical and chemical transformation due to the proximity of the water with the land surface. Evaporation and dissolution of salts increase the TDS of these waters. Flow paths into the region have both a horizontal and vertical component to them. The presence of the 1800 km^3 evaporite deposits and corresponding brine provides a density contrast between this inflowing water and the brine causing the flow paths to converge on the Tilopozo region until they reach 1–

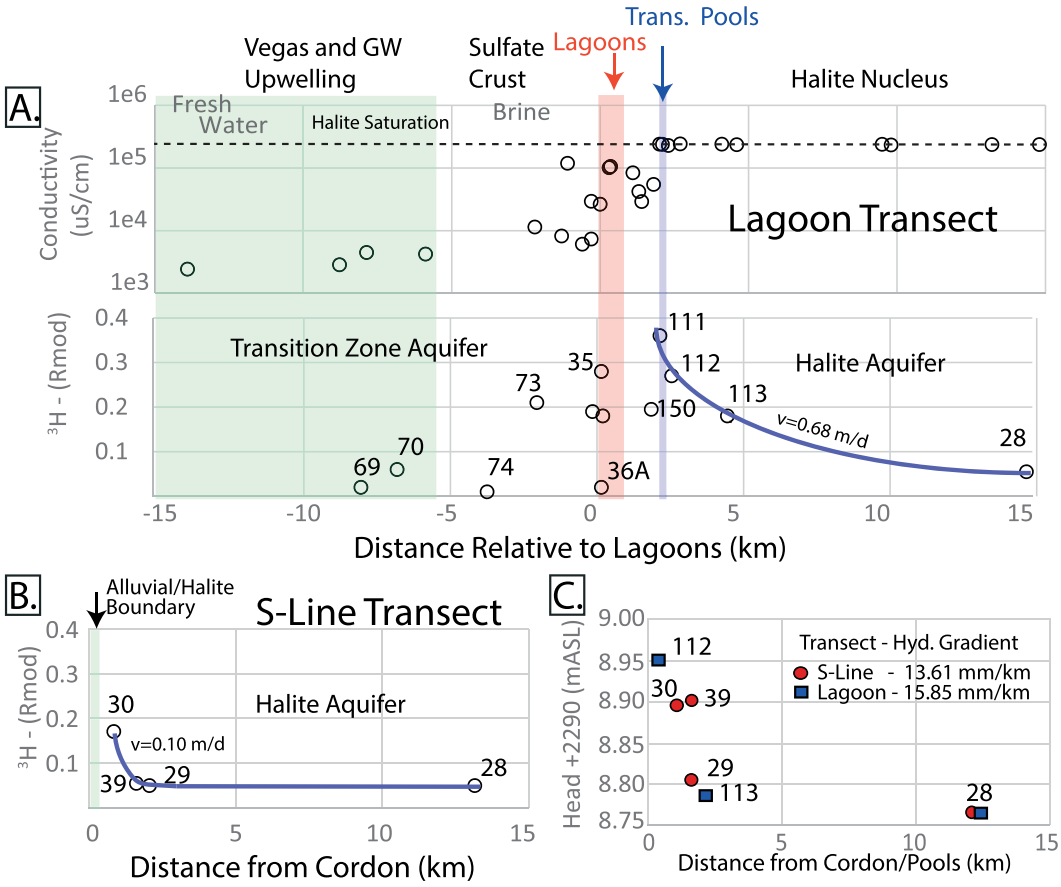

Figure 12. Transect of 3H concentration relative to modern precipitation (R_{mod}) for two transects, the lagoon transect (A) also showing water table specific conductivity. S-line transect 3H (R_{mod}) is depicted in B, no conductivity profile is shown because these samples are at halite saturation. Part C shows the hydraulic gradients in the observation wells from January 2014. The numbers next to symbols are sample IDs

2 m below ground surface. At this depth, evaporation begins to remove water from the system driving mineral precipitation in the order of calcite, gypsum, and halite, while Li concentrations increase in the residual waters. There are a number of discrete flow paths into the Tilipozo area that discharge at varying rates and locations throughout this transition zone (as evidenced by the variability of ^{3}H concentrations). This is to be expected as the geology of the aquifer system is spatially variable horizontally and vertically based on observations from 13 sediment cores taken in the transition zone up to 90-m depth. Some of the springs discharge at rates greater than the rate at which evaporation can remove the water into the atmosphere, forming small surficial water features. Water does not pool everywhere on the surface in this zone for two reasons: (1) discharge is less than the ET and (2) once the water is present at the surface ET, rates increase substantially resulting in a non-linear feedback. Because ET rates vary seasonally, some of these seeps with lower inflow rates form small lagoons that are ephemeral. The predominant discharge locations occur in the regions that are hydraulically up-gradient from the Punta/Brava lagoon complex. This lagoon complex is supported by discharge rates that greatly exceed ET forming large perenial surface water features. While there are local seeps in and around the margin of Punta/Brava lagoons, the majority of water flux into the lagoons appears to be up-gradient of the actual surface water features and is associated with surficial and shallow subsurface deposits indicative of discharge including carbonate mounds, carbonate muds, and diatomites. Satellite imagery and geochemical and isotopic analyses (not shown) of lagoon waters indicate that the lagoons are dynamic features that grow and shrink seasonally. Lagoon extent changes by over 400% over on an annual cycle due to changes in incident solar radiation. During the austral summer, solar radiation fluxes exceed discharge rates generating significant ET flux leading to the isotopic enrichment of the lagoon waters and increases in all dissolved phase species. Lagoons grow and expand seasonally, but also receive waters from the infrequent precipitation events on and around the transition zone.

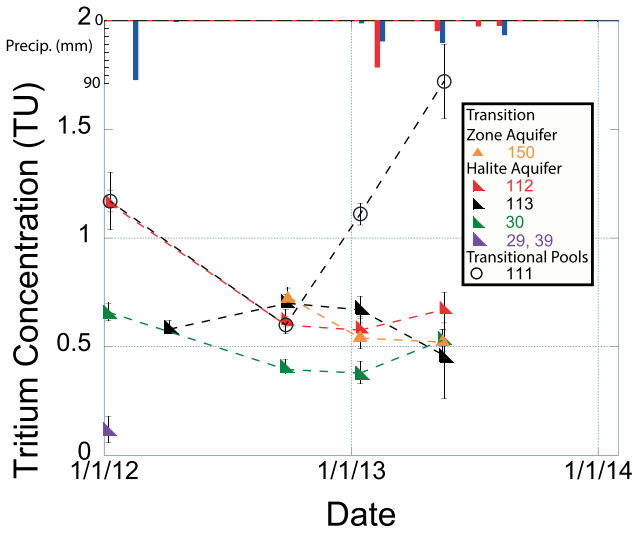

Figure 13. Time series during the study period of TU concentration of water samples from transitional pools and wells located in the transition zone and halite aquifer. Precipitation events shown for reference

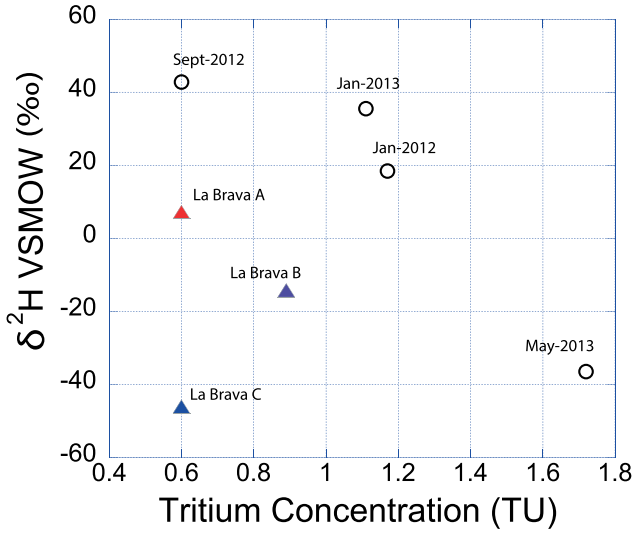

Figure 14. Crossplot of δ^2H–H^{2}O (VSMOW) *versus* tritium concentration (TU) for site 111 transitional pool samples and tritium samples for three Laguna La Brava points

Waters sampled between the lagoons and edge of the halite aquifer are sourced from fresh modern precipitation emplaced during precipitation events. The salarward limit of open surface water is the transitional pools. The pools are the surface representation of the halite barrier that effectively limits the salarward movement of the freshwater interface. This barrier is both a physical and reactive chemical feature that exhibits localized salt dissolution/precipitation from the influx of dilute rainwater. As shown, these pools contain waters that vary significantly throughout the sampling period in lithium, δ^2H, and ^{3}H composition but are always at conductivity levels of brine and fluctuating at or near halite saturation (Figure 14). The lithium concentrations are used as a first-order indicator of dilution and concentration effects following precipitation events. Low δ^2H values and ^{3}H concentration greater than 50% of modern precipitation ($R_{mod} > 0.5$) demonstrate that these waters result from recent precipitation dissolving salt and then rapidly evaporating, concentrating, and eventually precipitating salts again. Diffuse runoff/rainwater enters the transitional pools with depleted isotopic composition, few solutes, and modern ^{3}H values; this water then dissolves salt and progressively evaporates, rapidly increasing in TDS, and moves into the halite aquifer. This highly evaporated water is being advected into the halite nucleus forming a plume of high δ^2H water that is more enriched compared with the mean production brine. The transport distance and extent of influx suggest that this process has been going on for at least 50 years. The observed tritium in brine decreases with distance from the open pools, indicating that much of the water near the edge of the halite nucleus in our study area is in fact modern, and not the regional groundwater found in the lagoons. The decay of tritium along these flow paths permits estimation of lateral flow rates from the open pools toward the salar centre.

Water budget of the halite aquifer

We provide diverse evidence that multiple geochemically and isotopically distinct pathways are fluxing fresh water into the halite aquifer. For the brine aquifer in the southern portion of the SdA, there appears to be mountain front flux of water that bypasses the high evaporation region of the transition zone. The eastern margin of SdA is also characterized by an extensive transition zone and lagoon complexes, and therefore may operate similarly. Salas *et al.* (2010) and Ortiz *et al.* (2014) both show that a small fraction (<5%) of the water entering the Chaxa lagoon system in the northeast part of the Salar becomes recharge to the halite aquifer brine.

There is abundant evidence that across the 1664 km^2 halite aquifer, water levels increase strongly response to local precipitation events (Supporting Information; SQM and (Arcadis), 2013). We present an analysis based on distributed observations of water level changes in brine to arrive at estimates of the effect of local precipitation events on the water budget of the halite aquifer. We utilize the extraction rates of brine in the halite aquifer as a way to estimate various components of the brine budget by comparing predicted and observed changes in head (h). While brine pumping began in 1984, our calculations consider a time period from 1 January 2000 to 1 January 2010 because of data availability. The

change in elevation head is related to the net change in brine volume (V) by $\Delta h = \frac{\Delta V}{S_y * A}$; where S_y is the aquifer specific yield and A is the surface area of the halite nucleus. S_y, V, and A are estimated from Sociedad Chilena de Litio Ltda (2009) and Houston *et al.* (2011). The change in total volume of brine is assumed to be described by

$$\Delta V_{Total} = V_{pumping} + V_{evaporation} + V_{brine\ \ recharge} + V_{shallow\ \ subsurface\ \ inflow}$$

This neglects the possible addition of water into the salar by migration of the brine/fresh water interface or deeper inflowing waters (Jordan *et al.*, 2002; Corenthal *et al.*, in press). The change in water level in response to precipitation events multiplied by the S_y of the upper several metres of the nucleus provides estimates of direct recharge ($V_{brine\ \ recharge}$) envisaged through the mechanisms described in this paper. Evaporation rates in the nucleus are compiled from Mardones (1986) and Kampf and Tyler (2006), and pumping rates and estimates of shallow subsurface inflow are provided by Sociedad Chilena de Litio Ltda (2009).

From 2000 to 2010, observed brine levels over the whole aquifer with an area of 1664 km^2 (Figure 1) declined a net average of 0.3 m – consistent with the data presented in Figure 2 (see the Supporting Information for the plots of water level changes in other areas of the salar; SQM and (Arcadis), 2013). Furthermore, the net head decline includes responses to recharge from precipitation, so therefore represents a conservative estimate of potential decline from the removal of brine during this time period. Estimates of the specific yield (S_y) of the brine aquifer range from 18% near ground surface to 3% at depth of 40 m based on pumping tests (Sociedad Chilena de Litio Ltda, 2009) (localized areas of higher S_y are likely in a salt aquifer). Pumping of brine from 2000 to 2010 by both mining companies operating in SdA totalled 0.22 km^3, equivalent to an average of 0.7 m^3/s ($V_{pumping}$)over the 10-year time period (Sociedad Chilena de Litio Ltda, 2009).

Brine levels are shown to increase in level due to three major precipitation events in March 2001, March 2002, and February 2003 and across the whole salar (Supporting Information). We multiply the change in level from these precipitation events in 14 observation wells by a specific yield of 5.5% to calculate a total of 0.2 m^3/s of recharge to the brine aquifer ($V_{brine\ \ recharge}$) during the period 2000–2010.

Evaporation rates in the nucleus range from 0.005 mm/day (0.1 m^3/s) (Mardones, 1986) to below detection limit of <0.1 mm/day (Kampf and Tyler, 2006). Industry conceptual models (e.g. Sociedad Chilena de Litio Ltda, 2009) due include 0.1 m^3/s of shallow subsurface inflow from the transition zone to balance the evaporation from the nucleus.

Based on the earlier estimates, the brine volume from 2000 to 2010 changed by −0.6 m^3/s with a conservative uncertainty range from −0.7 to 0.1 m^3/s (Table V). An intermediate estimate for predicted head decline in the nucleus is 2.0 m, which is much larger than the net observed decline of 0.3 m. Specific yield plays a doubly important role in these calculations as it impacts the calculation of the magnitude of local precipitation into the salar and the resulting estimate of how much the head will change due to fluid extraction. Regardless of the choice of specific yield, the local recharge component to the halite aquifer is an important and essential component of the water budget. If all other parameters are held constant and no other inflow sources are included (such as deeper groundwater flow), a specific yield of 15% balances the observed inputs and outputs from 2000 to 2010 and matches the observed head declines. In this scenario, local influx into SdA is a critical component to the modern water budget of the SdA. Importantly, this water is generally lithium-poor compared with brine; thus, while this influx is important for the brine water budget, it does not serve as a significant component the mass budget of lithium.

Conceptual models of recharge in the Atacama Desert suggest that groundwater recharge only occurs in areas that receive over 120 mm/year or during intense precipitation events (Houston, 2009; Uribe *et al.*, 2015). The salar surface on average receives only ~16 mm of precipitation on an annual basis, yet we document that between 2012 and 2014; there was 47 mm of net recharge to the halite aquifer (between 2000 and 2010, it was 8.2 mm/year) assuming an S_y of 12%. A primary reason for this is that many regions of the Atacama Desert with similar precipitation rates have much deeper water tables (>100 m) than the basin floor of SDA. The high water table (<2 m to the surface) of SdA supported by the presence of the transition zone and the halite deposit itself allows a rapid flux of water to the water table – thereby bypassing thick vadose zone where water loss to ET can be high. As shown in the work of Kampf and Tyler (2006), evaporation off the halite aquifer is very small due to the fact that the salt essentially seals itself under the strong solar radiation along the Tropic of Capricorn. Whereas during precipitation events, salt dissolution enables the infiltration of water through the salt crust to the water table and eventually re-seals itself leading to recharge. Thus, on the basin floor, recharge events on or adjacent to the margin can yield infiltration rates of up to 50% of the precipitation amount compared with significantly lower rates watershed and region wide.

Table V. Modern water budget of halite aquifer system.

	Best estimate	Lower bound	Upper bound
Specific yield of upper 3 m (%) (Houston, 2011)	5.5	3	18
IN: Recharge from precipitation (m^3/s) [mm/year]	0.2 [3.75]	0.1 [2.05]	0.7 [12.3]
IN: Shallow subsurface inflow (m^3/s) [mm/year]	0 [0]	0 [0]	0.1 [1.86]
OUT: Brine pumping (m^3/s) [mm/year]	−0.7 [−13.1]	−0.7 [−13.8]	−0.7 [−12.5]
OUT: Evaporation (m^3/s) [mm/year]	−0.1 [−1.83]	−0.1 [−2.19]	0 [0]
NET CHANGE in brine flux (m^3/s)	−0.6 [−11.2]	−0.7 [−13.9]	0.1 [1.68]
Observed change in brine level (m)	−0.3 [−300] (Averaged across 1664 km^2 nucleus)		
Predicted change in brine level (m)	−2.0 [−2000]	−4.6 [−4600]	0.1

CONCLUSIONS

During the month of February in 2012 and 2013, two events delivered precipitation adjacent to and on the SdA basin floor. Precipitation events on the basin floor are rare compared with those in the main recharge area (the Altiplano–Puna plateau); we document that the recharge of water to the halite aquifer of SdA is partly sourced from these local precipitation events – and not completely from regional groundwater flow off the Altiplano. Large variations in the amount of evaporation of brine in the halite aquifer is observed and can be explained by considering distinct recharge pathways of water to the halite aquifer. The halite aquifer, which hosts an economically significant lithium brine, has a component of modern water and is replenished during infrequent but common precipitation events both on the salar itself and the surrounding alluvial fans. The halite/transition zone aquifers are dynamic systems that respond distinctly to short-term and long-term variations in precipitation and recharge regimes. Water discharging on the SdA basin floor (lagoons and vegas) is an integrator of diverse pathways of water that can only be understood by using multifaceted physical and geochemical tools to decipher pathways and transit times. Despite characterizing these modern pathways, there is still an unaccounted source of water into the brine aquifer that may be related to flux into the system from deep groundwater or the migration of the freshwater/brine interface.

ACKNOWLEDGEMENTS

The authors thank Rockwood Lithium (Albemarle) for their ongoing support of research on the origin of lithium brines and for the ability to publish data related to this work. The University of Utah Dissolved and Noble Gas Lab is thanked for their attention to generating the highest quality tritium data possible; Alan Rigby provided invaluable assistance in the field and lab, Wil Mace built a distillation apparatus for the brines, and Kip Solomon provided many useful discussions regarding tritium in South American hydrologic systems. Analyses of lithium in halite were supported by the United States National Science Foundation.

REFERENCES

Anderson M, Low R, Foot S. 2002. Sustainable groundwater development in arid, high Andean basins. *Geological Society London Special Publications* **193**(1): 133–144. DOI:10.1144/GSL.SP.2002.193.01.11

Aron F, González G, Veloso E, Cembrano J. 2008. Architecture and style of compressive Neogene deformation in the eastern-southeastern border of the Salar de Atacama Basin (22°30'-24°15'S): A structural setting for the active volcanic arc of the Central Andes. *International Symposium on Andean Geodynamics* (1998), 52–55.

Bookhagen B, Strecker MR. 2008. Orographic barriers, high-resolution TRMM rainfall, and relief variations along the eastern Andes. *Geophysical Research Letters* **35**(6): DOI:10.1029/2007GL032011

Clark ID, Fritz P. 1997. *Environmental isotopes in hydrogeology*. CRC Press/Lewis Publishers: Boca Raton, FL; 1–328.

Clarke WB, Jenkins WJ, Top Z. 1976. Determination of tritium by mass spectrometric measurement of ^{3}He. *International Journal of Applied Radiation and Isotopes* **27**: 515–522.

Correnthal LG, Boutt DF, Hynek SA, Munk L. 2016. Regional groundwater flow and accumulation of a massive evaporite deposit at the margin of the Chilean Altiplano. *Geophysical Research Letters* **43**. DOI:10.1002/2016GL07006

Dirección General de Aguas. 2013. Análisis de la Oferta Hídrica del Salar de Atacama, Santiago, Chile.

Eugster HP. 1980. Geochemistry of evaporitic lacustrine deposits. *Annual Review of Earth and Planetary Sciences* **8**(1): 35–63. DOI:10.1146/annurev.ea.08.050180.000343

Garreaud R, Vuille M, Clement AC. 2003. The climate of the Altiplano: observed current conditions and mechanisms of past changes. *Palaeogeography Palaeoclimatology Palaeoecology* **194**(1–3): 5–22. DOI:10.1016/S0031-0182(03)00269-4

Godfrey LV, Jordan TE, Lowenstein TK, Alonso RL. 2003. Stable isotope constraints on the transport of water to the Andes between 22° and 26°S during the last glacial cycle. *Palaeogeography Palaeoclimatology Palaeoecology* **194**(1–3): 299–317. DOI:10.1016/S0031-0182(03)00283-9

Hartley AJ, Chong G. 2002. Late Pliocene age for the Atacama Desert: implications for the desertification of western South America. *Geology* **30**(1): 43–46. DOI:10.1130/0091-7613(2002)030<0043:LPAFTA>2.0.CO;2

Herrera C, Pueyo JJ, Sáez A, Valero-Garcés BL. 2006. Relationship of surface and groundwater in the region of the lake and ponds Chungará Cotacotani, northern Chile: an isotopic study. *Revista Geologica de Chile* **33**(2): 299–325. DOI:10.4067/S0716020820060002000005

Houston J. 2002. Groundwater recharge through an alluvial fan in the Atacama Desert, northern Chile: mechanisms, magnitudes and causes. *Hydrological Processes* **16**(15): 3019–3035. DOI:10.1002/hyp.1086

Houston J. 2006a. Evaporation in the Atacama Desert: an empirical study of spatio-temporal variations and their causes. *Journal of Hydrology* **330**(3-4): 402–412. DOI:10.1016/j.jhydrol.2006.03.036

Houston J. 2006b. The great Atacama flood of 2001 and its implications for Andean hydrology. *Hydrological Processes* **20**(3): 591–610. DOI:10.1002/hyp.5926

Houston J. 2007. Recharge to groundwater in the Turi Basin, northern Chile: an evaluation based on tritium and chloride mass balance techniques. *Journal of Hydrology* **334**(3–4): 534–544. DOI:10.1016/j.jhydrol.2006.10.030

Houston J. 2009. A recharge model for high altitude, arid, Andean aquifers. *Hydrological Processes* **23**(16): 2383–2393. DOI:10.1002/hyp.7350

Houston J, Butcher A, Ehren P, Evans K, Godfrey L. 2011. The evaluation of brine prospects and the requirement for modifications to filing standards. *Economic Geology* **106**(7): 1125–1239. DOI:10.2113/econgeo.106.7.1225

Johnson E, Yáñez J, Ortiz C, Muñoz J. 2010. Evaporation from shallow groundwater in closed basins in the Chilean Altiplano. *Hydrological Sciences Journal* **55**(4): 624–635. DOI:10.1080/02626661003780458

Jordan TE, Munoz N, Hein M, Lowenstein T, Godfrey L, Yu J. 2002. Active faulting and folding without topographic expression in an evaporite basin, Chile. *Bulletin Geological Society of America* **114** (11): 1406–1421. DOI:10.1130/0016-7606(2002)114<1406:AFAFWT>2.0.CO;2

Jordan TE, Mpodozis C, Muñoz N, Blanco N, Pananont P, Gardeweg M. 2007. Cenozoic subsurface stratigraphy and structure of the Salar de Atacama Basin, northern Chile. *Journal of South American Earth Sciences* **23**(2-3): 122–146. DOI:10.1016/j.jsames.2006.09.024

Kampf SK, Tyler SW. 2006. Spatial characterization of land surface energy fluxes and uncertainty estimation at the Salar de Atacama, Northern Chile. *Advances in Water Resources* **29**(2): 336–354. DOI:10.1016/j.advwatres.2005.02.017

Magaritz M, Aravena R, Pena H, Suzuki O, Grilli A. 1990. Source of ground water in the deserts of northern Chile: evidence of deep circulation of ground water from the Andes. *Ground Water* **28**(4): 513–517. DOI:10.1111/j.1745-6584.1990.tb01706.x

Mardones L. 1986. Caracteristicas geologicas e hidrogeologicas del Salar de Atacama. In *El litio: Un nuevo recurso para CHile*, Lagos G (ed). Universidad de Chile: Santiago, Chile; 181–216.

Montgomery EL, Rosko MJ, Castro SO, Keller BR, Bevacqua PS. 2003. Interbasin underflow between closed Altiplano basins in Chile. *Ground Water* **41**(4): 523–531.

Munk, L.A., Hynek, S.A., Bradley, D.C., Boutt, D.F., Labay, K., Jochens, H. (2016). Lithium brines: a global perspective. Reviews in Economic Geology *v.* **18**, pp. 339-365. (R. Goldfarb, P.L. Verplanck, M. Hitzman, Eds.) Society of Economic Geologists.

Ortiz C, Aravena R, Briones E, Suárez F, Tore C, Muñoz JF. 2014. Sources of surface water for the Soncor ecosystem, Salar de Atacama basin, northern Chile. *Hydrological Sciences Journal* **59**(2): 336–350. DOI:10.1080/02626667.2013.829231

Pinder G, Bredehoeft J, Cooper H. 1969. Determination of aquifer diffusivity from aquifer response to fluctuations in river stage. *Water Resources Research* **5**(4): 50–855. DOI:10.1029/WR005i004p00850

Ramirez C, Gardeweg M. 1982. Carta Geologica de Chile, escala 1:250000, Hoja Toconao, Region de Antofagasta, Chile No. 54, Santiago, Chile.

Reutter K-J et al. 2006. The Salar de Atacama Basin : a subsiding block within the western edge of the Altiplano–Puna Plateau. *Andes: Active Subduction Orogeny* 303–325.

Reynolds R. 1987. Diffusivity of a glacial-outwash aquifer by the floodwave-response technique. *Ground Water* **25**(3): 290–299.

Rissmann C, Leybourne M, Benn C, Christenson B. 2015. The origin of solutes within the groundwaters of a high Andean aquifer. *Chemical Geology* **396**: 164–181. DOI:10.1016/j.chemgeo.2014.11.029

Rojstaczer S, Agnew DC. 1989. The influence of formation material properties on the response of water levels in wells to earth tides and atmospheric loading. *Journal of Geophysical Research: Solid Earth* **94** (B9): 12403–12411. DOI:10.1029/JB094iB09p12403

Rosen MR. 1994. Paleoclimate and basin evolution of playa systems, Geological Society of America Special Papers, Geological Society of America.

Salas J, Guimerà J, Cornellà O, Aravena R, Guzmán E, Tore C, Von Igel W, Moreno R. 2010. Hidrogeología del sistema lagunar del margen este del Salar de Atacama (Chile). *Bol. Geol. y Min.* **121**(4): 357–372.

Scanlon BR, Keese KE, Flint AL, Flint LE, Gaye CB, Edmunds WM, Simmers I. 2006. Global synthesis of groundwater recharge in semiarid and arid regions. *Hydrological Processes* **20**(15): 3335–3370. DOI:10.1002/hyp.6335

Sociedad Chilena de Litio Ltda. 2009. *Informe Hidrología e Hidrogeología Adenda 1 - EIA Modificaciones y Mejoramiento del Sistema de Pozas de Evaporación Solar en el Salar de Atacama.* Antofagasta: Chile.

SQM SA, Minera Escondida Ltda, Zaldívar CM, Sociedad Chilena de Litio Ltda. 2004. *Proyecto de Estudio y Monitoreo del Recurso Hídrico de la Cuenca del Salar de Atacama*. Antofagasta: Chile.

SQM SSA, (Arcadis) G. 2013. Informe No. 13 del Plan de seguimiento ambiental hidrogeologico proyecto cambios y mejoras de la operacion minera en el Salar de Atacama. No. 2013-245, Santiago, Chile.

Tyler SW, Muñoz JF, Wood WW. 2006. The response of playa and sabkha hydraulics and mineralogy to climate forcing. *Ground Water* **44** (3): 329–338. DOI:10.1111/j.1745-6584.2005.00096.x

Uribe J, Muñoz JF, Gironás J, Oyarzún R, Aguirre E, Aravena R. 2015. Assessing groundwater recharge in an Andean closed basin using isotopic characterization and a rainfall-runoff model: Salar del Huasco basin, Chile. *Hydrogeology Journal* **23**(7): 1535–1551. DOI:10.1007/s10040-015-1300-z

SUPPORTING INFORMATION

Additional supporting information may be found in the online version of this article at the publisher's web-site.